Am J Transl Res 2025;17(2):1237-1250
www.ajtr.org /ISSN:1943-8141/AJTR0160628

Original Article

Screening of RNA methyltransferase NSP16 inhibitors against SARS-CoV-2 coronavirus and study of related mechanisms

Xinyue Fan[1*], Dangui Zhou[1*], Chonghe Xu[2*], Xixi Song[1], Xin Wang[1], Chao Qin[1], Zhongqi Zhu[1], Wei Xu[3], Mei Zhu[1]

[1]Department of Clinical Laboratory, The Affiliated Chaohu Hospital of Anhui Medical University, Chaohu 238000, Anhui, PR China; [2]School of Basic Medical Sciences, Capital Medical University, Beijing 100069, PR China; [3]Department of Blood Transfusion, The First Affiliated Hospital of Anhui Medical University, Hefei 230022, Anhui, PR China. [*]Equal contributors.

Received September 19, 2024; Accepted January 18, 2025; Epub February 15, 2025; Published February 28, 2025

Abstract: Objective: We aimed to determine the abilities of several drugs to block the second methylation process of severe acute respiratory syndrome coronavirus 2 (SARS-CoV-2) RNA with non-structural protein 16 (NSP16) and expose the virus to the innate immune mechanism of the host for the purpose of improving infection control and drug development for COVID-19. Methods: Recombinant prokaryotic expression plasmids PET30a-NSP16 and PET15b-NSP10 and a plasmid for preserving the untranslated region (UTR) sequences, pUC57-UTR, were constructed. The obtained UTR template was transcribed in vitro to obtain RNAs. Then, bioluminescence was used to determine the K_m values of NSP16 and non-structural protein 10 (NSP10) and study the inhibition effects of four clinical drugs - cladribine, didanosine, sin efungin and ebselen - on SARS-CoV-2 NSP16 2'-O-MTase. Results: The catalytic subunit NSP16 and stimulatory subunit NSP10 of SARS-COV-2 2'-O-MTase were successfully expressed. The K_m values of the substrates of NSP16, including SAM and Cap0-RNA, were also determined. Among the four drugs, sinefungin exhibited the strongest inhibitory effect and ebselen ranked second, while cladribine and didanosine showed no significant inhibitory effects according to the luminescence data. Conclusion: Four drugs with potential inhibitory activity were examined. Among them, cladribine and didanosine have weak inhibitory effects on SARS-CoV-2 NSP16 and, therefore, are not suitable for clinical application. Sinefungin has the strongest inhibitory effect, and ebselen ranks second. Therefore, they can be regarded as qualified clinical candidates for SARS-CoV-2 treatment.

Keywords: SARS-CoV-2, NSP10, NSP16, RNA methyltransferase inhibitors, drug screening

Introduction

Severe acute respiratory syndrome coronavirus 2 (SARS-CoV-2) has caused one of the world's most severe pandemics. In late 2019, the first case of SARS-CoV-2 infection was documented in Wuhan, China. SARS-CoV-2 is highly infectious and causes severe viral pneumonia in a short period of time [1, 2]. Severe acute respiratory syndrome (SARS), MERS (Middle East respiratory syndrome) and SARS-CoV-2 had serious consequences in terms of their infectivity, severity and lethality within different time periods [3, 4]. SARS-CoV-2 has the largest genome among all single-stranded RNA viruses, containing 29,903 bases and encoding four structural proteins and 16 non-structural proteins (NSP1-NSP16) [5-7]. These proteins are involved in genomic RNA replication, subgenomic RNA transcription and other processes, such as the infection and colonization of SARS-CoV-2 [8-11]. Among them, both non-structural proteins 14 (NSP14) and 16 (NSP16) play irreplaceable roles in evading the innate immune system [12, 13].

The innate immune response is an important component of the human immune system. In order to survive, viruses have learned to evade the host's immune response [14, 15]. Since most of the intermediate products of SARS-CoV-2 replication are uncapped RNA fragments,

https://doi.org/10.62347/VUZM7431

they need to be modified via methylation at their ends to disguise themselves as mRNAs and evade immunosurveillance. Additionally, this can protect viral RNAs from exogenous enzymes and immune attacks from the host [16]. This coronavirus has two types of RNA MTases: NSP14 (N7-MTase) and NSP16 (2'-O-MTase), which are key enzymes in the first and second methylation processes, respectively. With the help of other enzymes, they can ensure the integrity of the capping process and methylate the 5' end of the RNA. In the methylation process, NSP10 serves as an activator that can not only enhance the catalytic activity of NSP16 but also activate NSP14 to exhibit its exonuclease activity [17].

Various small-molecule inhibitors of SARS-CoV-2 NSP16 2'-O-MTase have been discovered through various in vitro methods [18, 19]. In this study, we selected four drugs: cladribine, didanosine, sinefungin and ebselen. Cladribine is widely used in the treatment of hematological tumors [20, 21], multiple sclerosis [22] and myasthenia gravis [23]. As a commonly used chemotherapy drug in clinics, it is easy to obtain and generally does not have an inhibiting effect on methyltransferase, so it could be used as a negative control in these experiments. As anucleoside analogue, didanosine can serve as an HIV reverse transcriptase inhibitor (NRTI) and has a good therapeutic effect [24]. In a computer simulation screening of NSP16 [25], didanosine showed its potential as an inhibitor thereof due to its molecular structure, which is similar to that of s-adenosylmethionine (SAM). As a pan-inhibitor for methyltransferase, sinefungin can competitively inhibit the MTase activity and proliferation of the virus due to its similar structure to SAM [26]. After the outbreak of SARS-CoV-2, the inhibitory effect of sinefungin on NSP16 was confirmed by relevant research [27, 28]. Therefore, it could be used as a positive control. Ebselen is an organic selenium compound that can react with a variety of proteins to produce mercaptan, form selenium-sulfur bonds and change protein activity, therefore giving it antiviral activity [29]. Ebselen is a proven small-molecule capsid inhibitor of HIV-1 replication [30]. Additionally, early in the SARS-CoV-2 epidemic, it was considered to serve as an inhibitor of the SARS-CoV-2 capsid protein [31] and proven to have a good inhibitory effect on NSP14 [27]. Additionally, considering that both NSP14 and NSP16 have RNA methyltransferase activity, ebselen may also have an inhibitory effect on NSP16.

The MTase-Glo™ Assay employed in this research represents a bioluminescence-based method designed to identify inhibitors of 2'-O-methyltransferase (2'-O-MTase). This assay is pivotal for monitoring the enzymatic production of s-adenosyl-homocysteine (SAH), a byproduct indicative of methyltransferase activity. By detecting fluctuations in methyltransferase activity, it facilitates the screening of potential inhibitors that may disrupt this enzymatic function. Furthermore, its versatility allows for the evaluation of other types of protein methyltransferases, providing insights into their specificity and substrate requirements. Upon completion of the methyltransferase reaction, MTase-Glo™ Reagent is introduced to catalyze the conversion of SAH to adenosine diphosphate (ADP). Subsequently, MTase-Glo™ Detection Solution converts the ADP to adenosine triphosphate (ATP), allowing for the quantification of luminescence via the luciferin-luciferase reaction, which serves as a direct measure of methyltransferase activity.

This study is dedicated to exploring and inhibiting a critical step in the viral RNA capping process: secondary methylation, which is essential for augmenting the stability of viral transcripts and facilitating the expression of the proteins encoded by them within human cells infected by viruses. By targeting and inhibiting this specific methylation step, our research aimed to identify novel antiviral therapeutic targets, which are instrumental in the development of innovative antiviral strategies, offering a new paradigm for treating viral infections. This approach not only aimed to diminish the efficacy of viral replication within the host but also enhanced our understanding of the molecular mechanisms governing viral gene expression.

Materials and methods

Protein expression and purification

Related plasmid synthesis: The SARS-CoV-2 NSP10 and NSP16 sequences were obtained from the NCBI Virus database and were inserted into pET-15b and pET-30a vectors, respec-

tively. Then, the recombinant plasmids were successfully constructed, and the recombinant plasmids with different resistance genes were transformed into BL21 (DE3) for long-term preservation.

Expression and purification of NSP10 and NSP16: The cells mentioned in Section 2.1.1 (BL21 cells) were cultured overnight and induced with or without isopropyl-beta-d-thiogalactoside (IPTG) (0.1 mM). Subsequently, the harvested cells were resuspended in a lysis buffer and subjected to sonication and disruption under ice-cold conditions to ensure optimal cell lysis and extraction of intracellular components. Subsequent to purification using Ni-NTA agarose (Macherey-Nagel), the proteins were eluted, followed by desalination and concentration through ultrafiltration centrifugation and subsequent storage for future analysis. The samples derived from each elution phase were equilibrated with a corresponding volume of sample buffer marker prior to separation by means of polyacrylamide gel electrophoresis (SDS-PAGE). Post-electrophoresis, the gels either underwent Coomassie Brilliant Blue staining or were prepared for membrane transfer. The Coomassie was destained following a four-hour period, continuing overnight, whereas the membrane transfer entailed a two-hour milk block and a subsequent, brief C rinse before a 4°C overnight incubation with His-label mouse monoclonal antibodies (1:5000 dilution). Extensive washing was employed to eliminate any residual antibodies and minimize background interference. Sheep anti-mouse IgG HRP antibodies (1:5000 dilution) were then incubated at the ambient temperature for two hours. Following this, excess antibodies were removed, and a luminescent detection solution - comprising equal parts of solutions A and B - was applied uniformly across the protein membrane to facilitate imaging. The resultant images were meticulously recorded and subjected to detailed analysis.

Synthesis of RNA products targeted by 2'-O-MTase

Related plasmid synthesis: The SARS-CoV-2UTR sequence (from NCBI) was inserted into pUC57. The complete plasmid containing this sequence was shifted to DH5α for long-term preservation.

Plasmid extraction and enzyme digestion: Plasmids were extracted from DH5α cells with the SARS-CoV-2 UTR sequence using the Plasmid Mini-Extraction Medium Volume Kit (code no. DP106-02; TIANGEN, China). Then, the plasmids were sufficiently linearized via single-enzymatic cleavage with the BspQI enzyme (code no. R0712S; NEB, America) to obtain the target templates. Next, the templates were amplified by using PCR with KOD One™ PCR Master Mix (code no. KMM-101; TOYOBO, Japan).

Purification of PCR products: The PCR products were subjected to AGE (agarose gel electrophoresis) to assess the degrees of enzyme cleavage, and the gel blocks containing the target genes were recovered using the UNIQ-10 Column Micro Agarose Gel DNA Recovery Kit (code no. B511139-0050; Sangon Biotech, China).

In vitro transcription with T7 RNAP and DNase I treatment: In vitro transcription was performed using the High-Yield T7 RNA In Vitro Transcription Kit (code no. B639253-0050; Sangon Biotech, China). Then, the DNA templates were digested with RNase free DNase I (code no. 2270A; Takara, Japan) to obtain pure RNAs. RNase-free DNase I (15 U) was added and mixed into each transcription system (20 μl). The whole reaction system was incubated at 37°C and then at 75°C to deactivate the enzyme. Finally, it was immediately placed on ice for cooling.

Capping and purification of RNAs: The RNAs were purified after both the DNA template digestion and their first methylation using the Column Rapid RNA Concentration and Purification Kit (code no. B518688; Sangon Biotech, China). Additionally, the Vaccinia Capping System (code no. M2080S; NEB, America) was used to add 7-methylguanylate cap structures (Cap-0) to the 5' end of each RNA generated by in vitro transcription and targeted by 2'-O-MTase.

Chemicals and assay components: The MTase-Glo™ Methyltransferase Assay Kit (code no. V7601; Promega Corporation, America) contains SAH, SAM, MTase-Glo™ Reagent and MTase-Glo™ Assay Solution. Four drugs were involved: cladribine, didanosine, sinefungin and ebselen (code nos. HY-13599, HY-

B0249, HY-101938 and HY-13750; MedChemExpress, America). In the following experiments, all four drugs were used in the form of solutions, of which sinefungin was soluble in water and the other three drugs were soluble in DMSO (dimethyl sulfoxide).

SAH standard curve: The SAH standard curve was generated to assess the linearity of determinations during enzyme titrations and to correlate SAH concentration and luminescence. A total of 1 μM SAH solution was prepared in advance. In a 96-wellplate, 150 μL of this solution (1 μM) was serially double-diluted from wells A1 to A11. Then, 75 μL of the dilution in well A11 was discarded, while well A12 contained only 75 μL of 1× reaction buffer. In each of the 12 wells, 20 μL of solution was transferred to the analytical plate. A total of 5 μL of 5× MTase-Glo™ Reagent was added to each well and mixed. The mixture was incubated for 30 min. Then, 25 μL of MTase-Glo™ Assay Solution was added to all wells and mixed again. After that, the wells were incubated at room temperature for 30 min for a luciferase-luciferin reaction. The luminescence of three replicate experiments was measured, and the data were recorded.

Verification of enzyme activity of NSP16 2'-O-MTase: The properties of the MTase had to be verified in advance. The reaction was carried out in a 20 μL mixture, with RNA and serial twofold dilutions of preformulated MTase solution added separately. Then, the mixture in each reaction system was kept at 30°C for 1 h. After that, enzyme deactivation of the MTase was performed by raising the temperature. Then, 5 μL of 5× MTase-Glo™ Reagent, prepared in advance, was added to each well, mixed and incubated at room temperature for 30 min. After that, 25 μL of MTase-Glo™ Assay Solution was added to all wells and incubated at room temperature for 30 min for the luciferase-luciferin reaction. The luminescence of three replicate experiments was measured, and the data were recorded.

K_m values for substrates of NSP16: After the validation of the properties of NSP16 2'-O-MTase, the K_m values of the SAM and Cap0-RNA were determined. We separately prepared 0.5% trifluoroacetic acid, 6× MTase-Glo™ Reagent, the substrate dilution buffer for the SAM and Cap0-RNA, the enzyme solution of twice the final concentration and the SAM solution and Cap0-RNA solution of fixed-concentration gradients (from 1 μM to 8 μM). The concentration of the substrate solution was adjusted with the substrate diluent buffer. Then, 10 μL each of the mixture and enzyme solution were added to the corresponding wells, respectively. After that, the temperature was adjusted to 30°C for 1 h to allow a full methyltransferase reaction. Subsequently, the temperature was raised to 75°C for 10 min to deactivate the enzyme. After the methyltransferase reaction system was cooled to room temperature, 5 μL of 6× MTase-Glo™ Reagent, at room temperature, was added to all wells. The mixture was incubated for 30 min. Then, 5 μL of 0.5% trifluoroacetic acid was added to stop the reaction. The mixture was further incubated at room temperature for 5 min. Finally, 30 μL of MTase-Glo™ Assay Solution was added and mixed. Afterward, these were kept at ambient temperature once again for 30 min. The luminescence of three replicates of the experiment was measured, and the data were recorded.

ADMET prediction method: The SMILES sequences of four drugs - cladribine, didanosine, sinefungin and ebselen - were obtained from PubChem. After the sequences were checked, the SMILES sequence numbers were uploaded into ADMETlad 2.0 to predict the relevant properties and data.

Inhibitor studies involving the MTase-Glo™ assay: The relevant solutions were prepared in advance, including 2.5 μM SAM solution and four kinds of drug solutions containing cladribine, didanosine, sinefungin and ebselen, respectively. The enzyme complexes were prepared with Cap0-RNA as a substrate. As a result, each reaction system contained 2.0 μM NSP16, 16.0 μM NSP10, 0.7 μM Cap0-RNA and 2.5× MTase-Glo™ Reagent. Serial twofold dilutions of the drugs were performed, and a reaction buffer was used as the blank control in the test. We added 5 μL of each drug solution to the appropriate well. Then, 10 μL of the prepared enzyme complex was added to each well and incubated for 10 min. After that, 10 μL of 2.5 μM SAM was added to allow the methyltransferase reaction. Finally, 25 μL of MTase-Glo™ Assay Solution, at room temperature, was added to all wells. The reacting sys-

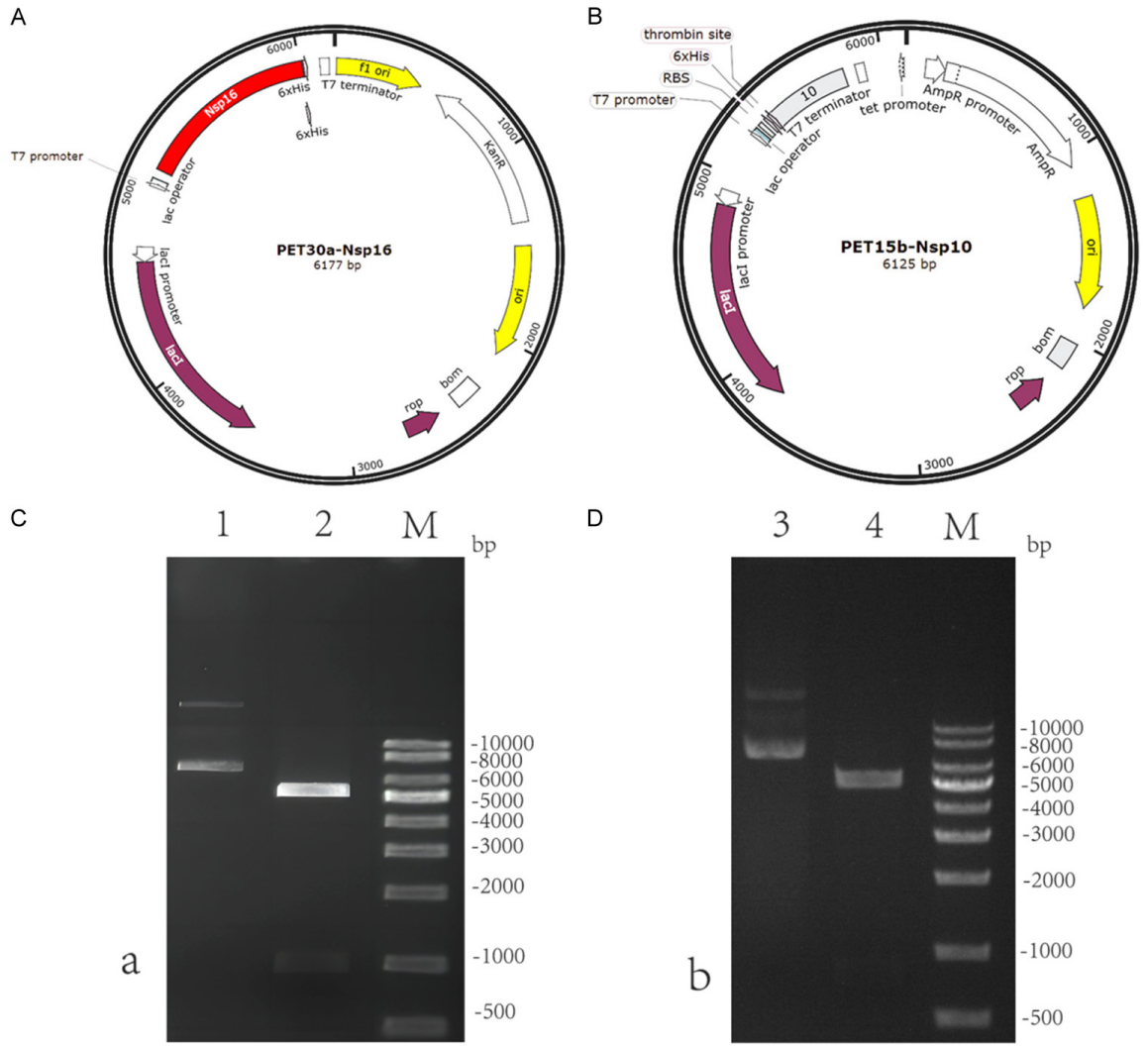

Figure 1. Identification of NSP10 and NSP16. A. PET30a-NSP16: recombinant plasmid for NSP16. B. PET15b-NSP10: recombinant plasmid for NSP10. C. Identification of NSP16 recombinant plasmids via enzyme digestion: Lane 1, PET30a original plasmid electrophoresis; Lane 2, electrophoresis using NcoI and ClaI digestion; Lane M, marker; and a, inserted NSP16 fragment (936 bp). D. Identification of NSP10 recombinant plasmids via enzyme digestion: Lane 1, PET15b original plasmid electrophoresis; Lane 2, electrophoresis using NcoI and ClaI digestion; Lane 3, marker; and b, inserted NSP10 fragment (784 bp). Each experiment was replicated thrice to ensure the reproducibility and robustness of the findings.

tem was kept at room temperature for 1 h. Upon completion of all reactions, the luminescence of three replicated experiments was measured and the data were recorded.

Signal detection and data analysis: Plotting, data analyses and calculations of the biochemical parameters of the MTases were performed using Microsoft Excel and Prism from GraphPad Software. IC_{50} values were determined by means of non-linear regression using a fitted S-shaped dose response (variable slope).

Results

Successful expression of NSP10 and NSP16

Recombinant plasmids PET30a-NSP16 (**Figure 1A**) and PET15b-NSP10 (**Figure 1B**) were preliminarily identified by means of PCR and the double-enzyme digestion reaction. The fragment sizes of the enzyme digestion products of PET30a-NSP16 (**Figure 1C**) and PET15b-NSP10 (**Figure 1D**) were consistent with the sizes of their inserted fragments, as the sequencing results of those products were with

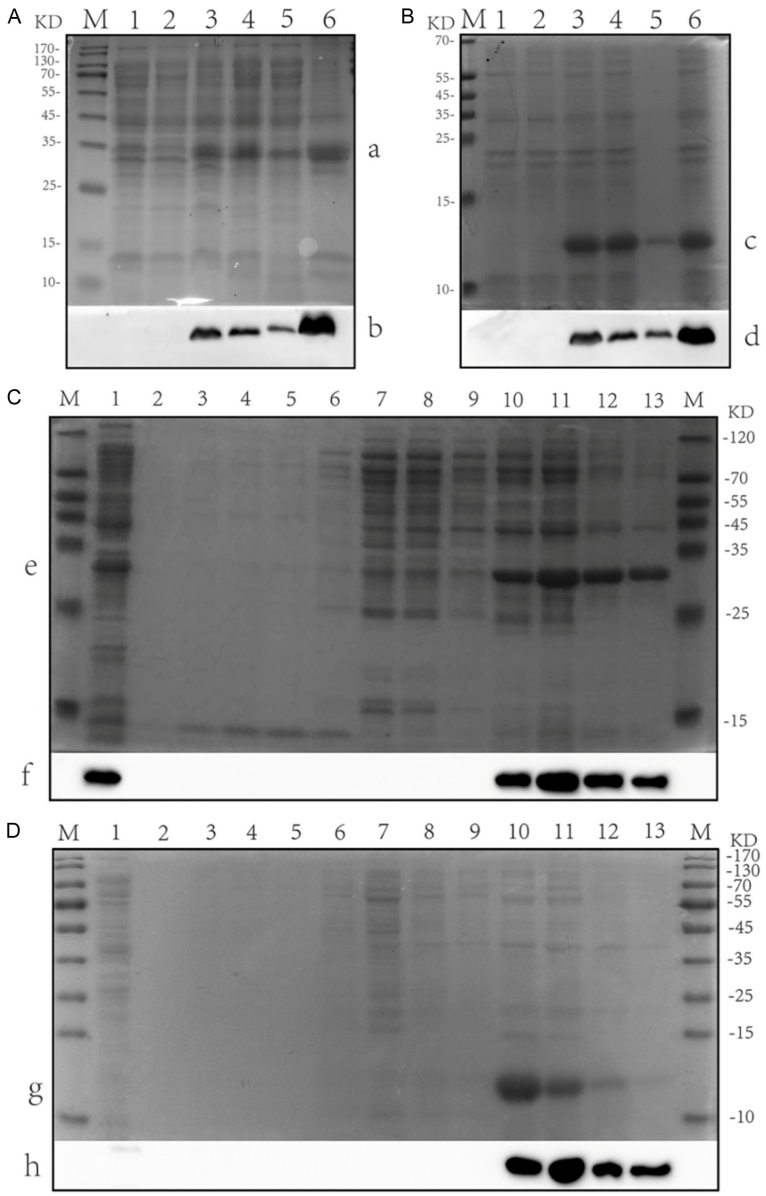

Figure 2. Identification of expressed proteins. A. The ultrasonic crushing of NSP16 (34.16 kD) was carried out under the best conditions. Lane M, marker; Lane 1, before induction; Lane 2, after induction and before lysis; Lane 3, after lysis; Lane 4, whole-cell fluid after ultrasound; Lane 5, cell supernatant after ultrasound; Lane 6, cell precipitation after sonication. B. The ultrasonic crushing of NSP10 (15.62 kD) was carried out under the best conditions. Lane M, marker; Lane 1, before induction; Lane 2, after induction and before lysis; Lane 3, after lysis; Lane 4, whole-cell fluid after ultrasound; Lane 5, cell supernatant after ultrasound; Lane 6, cell precipitation after sonication. C. NSP16-related identification: Lane M, marker; Lane 1, flow-through solution; Lanes 2-5, lysis buffer elution; Lanes 6-9, 20 mM imidazole elution; and Lanes 10-13, 250 mM imidazole elution. a and c: SDS-PAGE electrophoresis of the target protein NSP16. b and d: Western Blot identification of the target protein NSP16. D. NSP10-related identification: Lane M, marker; Lane 1, flow-through solution; Lanes 2-5, lysis buffer elution; Lanes 6-9, 20 mM imidazole elution; and Lanes 10-13, 250 mM imidazole elution. e and g: SDS-PAGE electrophoresis of the target protein NSP10. f and h: Western Blot identification of the target protein NSP10. Each experiment was replicated thrice to ensure the reproducibility and robustness of the findings.

the published sequences. The optimal time and IPTG concentration to induce the protein were determined (23°C for 16 h with 0.1 mM IPTG). Proteins from different treatment stages were identified separately, such as before induction, after induction, before lysis, after lysis, whole-cell fluid after ultrasound, cell supernatant and cell precipitation. The proteins expressed by the plasmids could only be detected at least after cell lysis (**Figure 2A** and **2B**). The proteins attached to the nickel columns were cleaned and eluted with different concentrations of imidazole solutions (20 mM and 250 mM) to obtain purified proteins. After the nickel column chromatography, SDS-PAGE electrophoresis and Western Blot analysis were performed on those purified proteins. This study demonstrated successful expression of PET30a-NSP16 and PET15b-NSP10, which matched the target protein's molecular weight (**Figure 2C** and **2D**).

Preparation and modification of RNA substrates

The plasmid PUC57 template (**Figure 3A**) containing the cDNA fragment of the viral UTR sequence was digested, and the product was expanded by means of PCR. Then, the expanded DNA was subjected to AGE (**Figure 3B**). The digested target templates were recovered using the Gel DNA Recovery Kit. The DNA templates that met the condition of the ratio of A260/A280 being between 1.8 and 2.0 were used for the following experiments. Then, the substrate RNA was obtained via in vitro transcription. The

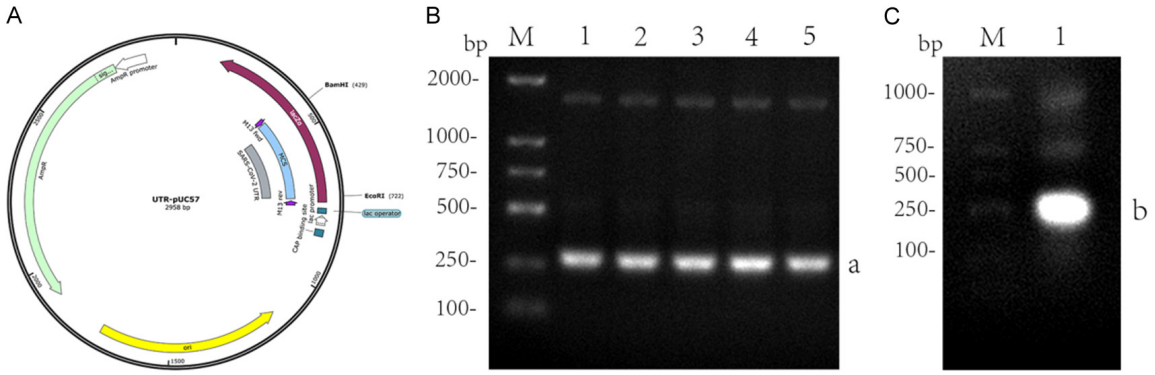

Figure 3. Agarose images of the target RNA and the target DNA. A. UTR-PUC57: recombinant plasmid for UTRs (untranslated regions). B. AGE (agarose gel electrophoresis) of PCR products: Lane M, marker; Lanes 1-5, PCR products; and a, UTR-DNA (259 bp). C. Denaturing agarose electropherogram of transcription products: Lane M, marker; Lane 1, transcription products; and b, UTR-RNA (259 nt). Each experiment was replicated thrice to ensure the reproducibility and robustness of the findings.

RNA was subjected to denaturing agarose electrophoresis (**Figure 3C**) to determine whether the product matched the expected single RNA. The Bovine Pox Plus Cap Kit was used to carry out the first methylation of the 5' end of the substrate RNA, transforming it into Cap0-RNA.

Determining whether NSP16 has 2'-O-MTase methyltransferase activity

SAM was used as the reaction substrate to methylate the Cap0-RNA with NSP16 and NSP16/NSP10, respectively. Moreover, the optimal concentration ratio of NSP16 to NSP10 was determined to be 1:8 (**Figure 4A**), which resulted in the maximum fluorescence signal. The SAH standards, prepared in each experiment, were proportional to the luminescence signals generated in the MTase-Glo™ Methyltransferase Assay (**Figure 4B-D**). As can be seen from the figures below, the enzyme activity of NSP16 was enhanced in the presence of NSP10, resulting in a greater catalytic effect than that of NSP16 alone. The difference between the two experiments indicates that NSP16 had 2'-O-MTase activity and NSP10 had a catalytic effect on it, which shows that the plasmid was constructed successfully (**Figure 4E**).

Determination of substrate K_m values for SARS-CoV-2 NSP16 2'-O-MTase

We evaluated the linear relationship between the initial velocities (activity vs. time) of different concentrations of Cap0-RNA and SAM at fixed concentration gradients. Their slopes were calculated and used to determine the kinetic parameters for NSP16 MTase activity. The K_m values of the substrates of NSP16 2'-O-MTase, including the SAM (1.992±0.575 μM) and Cap0-RNA (2.921±0.696 μM), were determined (**Figure 5**).

Drug screening targeting NSP16 2'-O-MTase

In small-molecule screening campaigns, typically, assays are performed at the K_m values of substrates to allow potential inhibitors to compete with them. However, in this experiment, we mainly monitored the formation of SAH, which can be used to detect changes in methyltransferase activity. Therein, sinefungin was used as a positive control while cladribine was used as a negative control. The NSP16 2'-O-MTase was very weakly inhibited by cladribine and didanosine in the MTase-Glo™ Assay. Even when the concentration of didanosine was increased to three orders of magnitude above the other drugs, the inhibitory effect remained weak. In contrast, sinefungin and ebselen had very significant inhibitory effects. Additionally, the IC_{50} value of sinefungin was lower than that of ebselen (**Figure 6**).

ADMET analysis

The main contents of ADMET analysis include (i) physicochemical properties, (ii) medicinal chemistry, (iii) absorption, (iv) distribution, (v) metabolism, (vi) excretion and (vii) toxicity. Sinefungin and ebselen potently inhibit SARS-

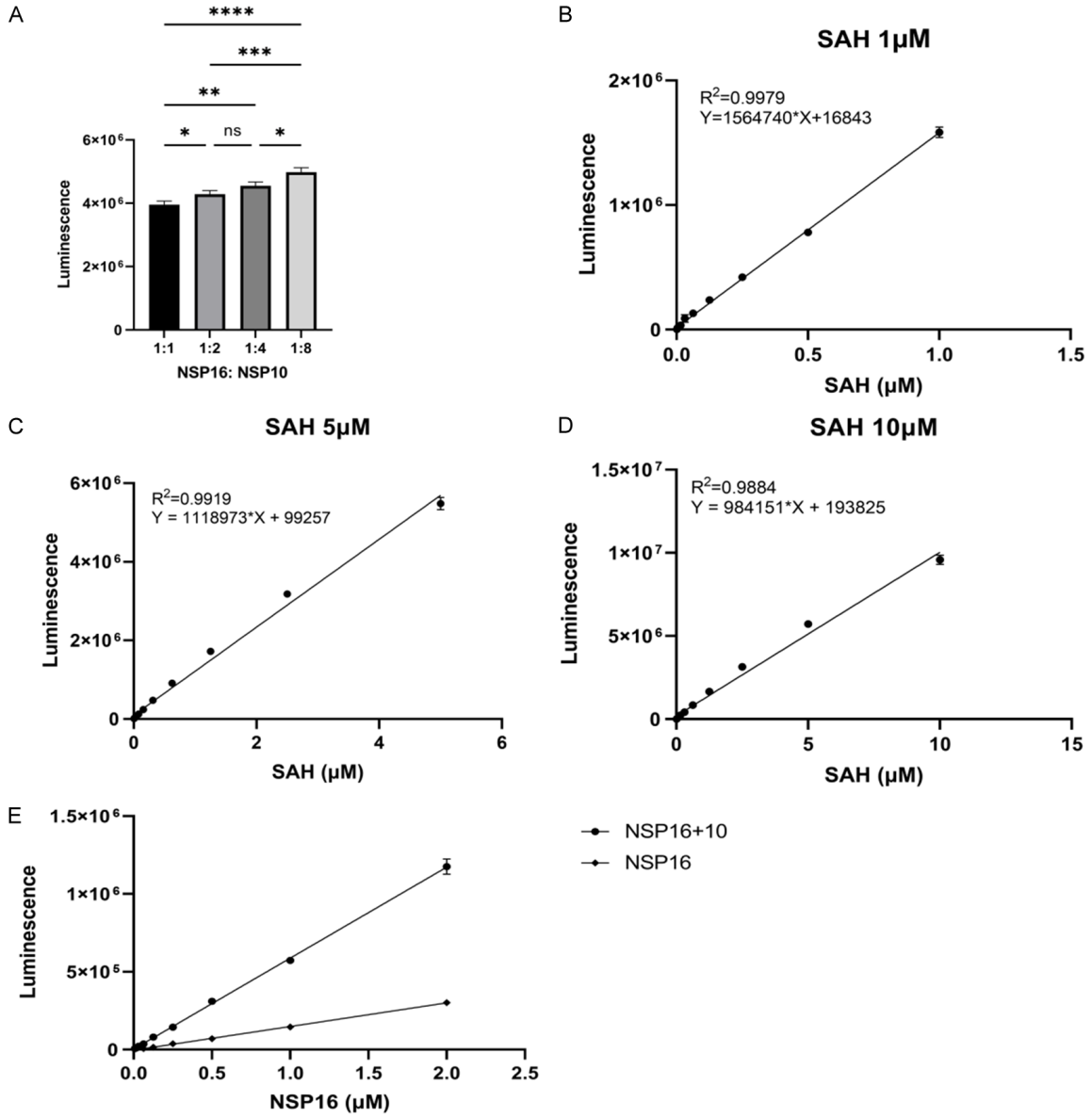

Figure 4. Property validation of NSP16 based on MTase-Glo™ Luminescence System. (A) Determined optimal stoichiometry of SARS-CoV-2 NSP16/NSP10 MTases. The concentration of NSP16 kept constant (2.0 μM), while the concentration of NSP10 gradually increased (2.0 μM, 4.0 μM, 8.0 μM, 16.0 μM). Reactions were carried out in a solid white low-volume 96-well plate for 60 min at 37 °C. The MTase-Glo™ Assay was performed as described in Materials and Methods. (B-D) These images show the standard curve of the luminescence detection system; all used a white 96-well plate with sufficient Cap0-RNA added to each reaction system. The labels "SAH (1, 5, 10 μM)" denote the apex concentrations employed in the gradient concentration curve assays. The abscissa in the accompanying graph delineates a spectrum of dilutions derived from these maximal concentrations, systematically exploring the dose-response relationship. (E) The image shows the data measured by adding NSP16/NSP10 or only NSP16 to each reaction system. The data in (A) were analyzed using one-way analysis of variance (ANOVA). Data are presented as means ± standard deviation (SD), with statistical significance denoted by asterisks (*P < 0.05, **P < 0.01, ***P < 0.001, ****P < 0.0001, ns = not significant). Each experiment was replicated thrice to ensure the reproducibility and robustness of the findings.

CoV-2 NSP16 with acceptable physicochemical properties. The biofilm penetration of ebselen is excellent, and it exhibited significant gut absorption. Sinefungin exhibited superior in vivo dissociation and permeability to the blood-brain barrier with minimal interference with the

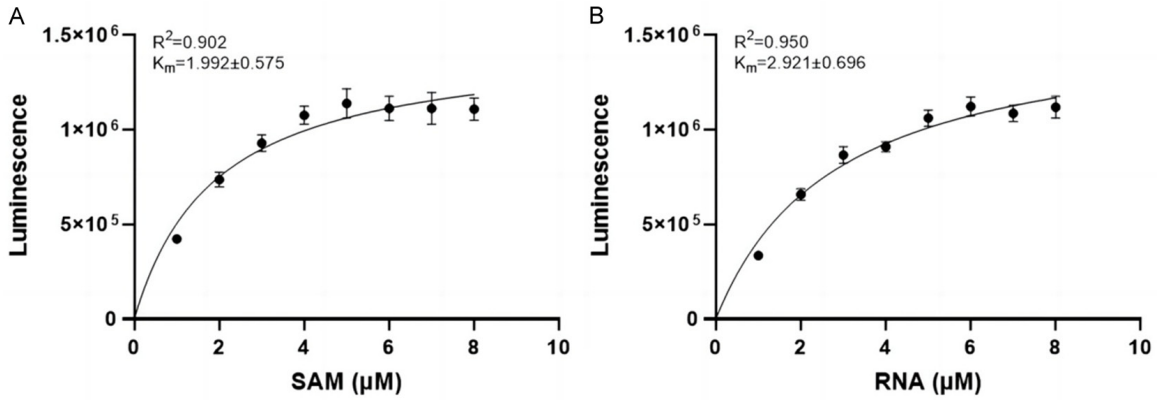

Figure 5. SARS-CoV-2 NSP16/NSP10MTase kinetic parameters. A. K_m value of SARS-CoV-2 NSP16 2'-O-MTase for SAM. B. K_m value of SARS-CoV-2 NSP16 2'-O-MTase for RNA. Each experiment was replicated thrice to ensure the reproducibility and robustness of the findings.

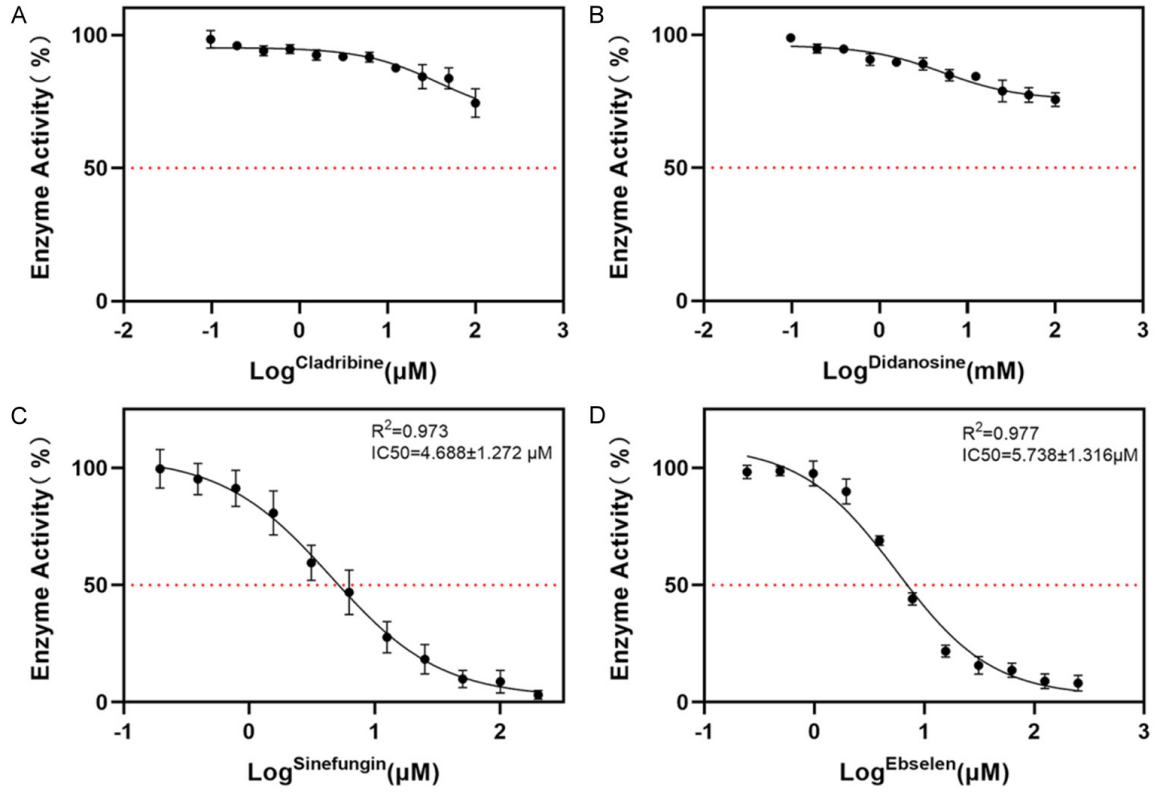

Figure 6. Screening for inhibitors of NSP16 2'-O-MTase: inhibition by (A) cladribine, (B) didanosine, (C) sinefungin and (D) ebselen. Each point is the mean of three technical repeats, with error bars indicating SD. Each experiment was replicated thrice to ensure the reproducibility and robustness of the findings.

cytochrome P450 metabolism in vivo. Ebselen inhibits CYP1A2, CYP2C19 and CYP2C9, which may significantly impact cytochrome P450 metabolism. The clearance of both drugs is considered acceptable; however, it should be acknowledged that both drugs carry a potential risk of respiratory and liver harm, as indicated in **Table 1**. The inhibitory effects of cladribine and didanosine on the SARS-CoV-2 NSP16 were not found to be superior; thus, their rele-

Table 1. Performance of the regression and classification models incorporated into the ADMET platform

Category	Model	Cladribine	Didanosine	Ebselen	Sinefungin
Physicochemical Property	Molecular Weight (MW)	285.06	236.09	274.98	381.18
	Volume	241.867	215.659	28731115.16	350.073
	Density	1.179	1.095	0	1.089
	nHA	8	7	2	12
	nHD	4	2	0	9
	nRot	2	2	1	7
	nRing	3	3	3	3
	MaxRing	9	9	9	9
	nHet	9	7	3	12
	fChar	0	0	0	0
	nRig	16	16	17	17
	Flexibility	0.125	0.125	0.059	0.412
	Stereo Centers	3	2	0	6
	TPSA	120.04	93.03	22	209.38
	logS	-1.606	-1.539	-3.336	-1.892
	logP	-0.871	-0.642	2.441	-3.891
	logD	0.006	-0.227	2.589	-1.278
Medicinal Chemistry	QED	0.556	0.752	0.622	0.276
	SAscore	4.182	3.611	2.567	4.635
	Fsp3	0.5	0.5	0	0.6
	MCE-18	60.067	53	14	66.667
	NPscore	0.732	0.677	-0.454	1.211
	Lipinski Rule	Accepted	Accepted	Accepted	Rejected
	Pfizer Rule	Accepted	Accepted	Accepted	Accepted
	GSK Rule	Accepted	Accepted	Accepted	Accepted
	Golden Triangle	Accepted	Accepted	Accepted	Accepted
Absorption	Caco-2 Permeability	-5.717	-5.553	-4.537	-6.261
	MDCK Permeability	1.20E-05	5.70E-06	2.00E-05	1.6E-05
	Pgp-Inhibitor	---	---	---	---
	Pgp-Substrate	-	+++	---	+++
	HIA	---	---	---	+++
	F20%	---	---	+++	-
	F30%	---	---	--	++
Distribution	PPB	21.03%	15.44%	93.18%	11.56%
	VD	7.267	0.982	0.435	0.571
	BBB Penetration	+	-	+	++
	Fu	68.49%	83.17%	5.01%	87.91%
Metabolism	CYP1A2 Inhibitor	--	---	+++	---
	CYP1A2 Substrate	+++	+++	+	---
	CYP2C19 Inhibitor	--	---	++	---
	CYP2C19 Substrate	---	--	-	---
	CYP2C9 Inhibitor	---	---	++	---
	CYP2C9 Substrate	---	++	+	---
	CYP2D6 Inhibitor	---	---	---	---
	CYP2D6 Substrate	---	---	-	--
	CYP3A4 Inhibitor	---	---	--	---
	CYP3A4 Substrate	--	---	++	---

Excretion	CL	11.614	11.587	1.678	3.097
	$T_{1/2}$	0.824	0.898	0.220	0.910
Toxicity	hERG Blockers	---	---	---	--
	H-HT	+++	+++	--	++
	DILI	+++	+++	++	+++
	AMES Toxicity	++	+++	++	--
	Rat Oral Acute Toxicity	-	--	---	---
	FDAMDD	++	+++	---	--
	Skin Sensitization	--	++	++	++
	Carcinogenicity	+++	++	++	--
	Eye Corrosion	---	---	---	---
	Eye Irritation	---	---	+++	---
	Respiratory Toxicity	+++	---	+++	+
	Bioconcentration Factors	0.158	0.032	1.305	-0.042
	IGC50	2.155	1.934	4.119	2.659
	LC50FM	3.635	2.178	4.73	2.821
	LC50DM	3.788	2.383	5.158	3.528
	NR-AR	---	---	---	---
	NR-AR-LBD	---	---	---	---
	NR-AhR	--	---	++	---
	NR-Aromatase	-	++	++	++
	NR-ER	---	---	++	--
	NR-ER-LBD	---	---	---	---
	NR-PPAR-Gamma	---	---	---	---
	SR-ARE	++	+	++	-
	SR-ATAD5	---	---	--	---
	SR-HSE	---	---	++	---
	SR-MMP	---	---	++	---
	SR-p53	+++	++	+	+

For the classification endpoints, the prediction probability values have been transformed into six symbols: 0-0.1 (---), 0.1-0.3 (--), 0.3-0.5 (-), 0.5-0.7 (+), 0.7-0.9 (++) and 0.9-1.0 (+++). Refer to Table S1 for detailed explanations of the endpoints under the model in this table.

vant characteristics have been summarized in **Table 1** (the explanation of the available endpoints of **Table 1** is given in Table S1).

Discussion

In this investigation, we evaluated the inhibitory effects of several drugs on SARS-CoV-2 NSP16 in vitro. Our findings indicate that cladribine lacks sufficient inhibitory efficacy at concentrations above the IC_{50} [32], thus deeming it unsuitable for clinical use as an effective inhibitor against SARS-CoV-2 NSP16. Similarly, didanosine failed to demonstrate significant inhibition even at elevated concentrations, leading us to advise against its clinical application for this purpose due to its limited efficacy and potential side effects [33, 34]. Conversely, sinefungin exhibited potent inhibition, underscoring its potential as a viable clinical candidate. Given its established profile as a broad-spectrum methyltransferase inhibitor, it not only presents a strong therapeutic opportunity but also serves as a foundation for the synthesis of analogues designed to mitigate adverse reactions. Ebselen also showed notable inhibitory effects; although its IC_{50} was higher and its inhibitory capacity lower than those of sinefungin, its extensive use in treating viral infections enhances its clinical relevance. However, the mechanisms by which it inhibits SARS-CoV-2 NSP16 remain to be fully elucidated. The preliminary data suggest that its activity may involve binding to protein residues, thereby impacting enzymatic function. It is important to note that the variations in the

IC_{50} values for sinefungin and ebselen as compared with those reported in other studies could be attributed to differences in the drug screening systems used. Our study also observed a minor inhibitory effect of cladribine at high concentrations, likely influenced by the cosolvent DMSO. This was similarly noted with didanosine, suggesting a potential cosolvent effect on enzyme activity. Despite these findings, the solubilization medium for sinefungin (DNase/RNase-free water) ensured that its inhibitory effects were not compromised by the DMSO. While the experimental results are promising, they come with inherent limitations. The stability of the bioluminescence signals might have been affected by the equipment used and external factors. Additionally, the interactions between the DMSO and protein components could have slightly skewed the bioluminescence readings.

We conducted an ADMET analysis of the four drugs using the ADMETlad 2.0 platform and demonstrated the pertinent properties of the two candidates with superior inhibition rates and their potential clinical applications. Considering that SARS-CoV-2 frequently induces nervous system damage in both adults and children [35, 36], the effective blood-brain barrier penetration of a drug to exert antiviral effects was also a focal point of our investigation. In line with our predictions, sinefungin exhibited enhanced blood-brain barrier permeability, thereby increasing its applicability in this context. Moreover, ebselen's predictive results indicate potent inhibitory effects on CYP1A2, warranting caution when co-administering it with drugs metabolized by CYP1A2, such as theophylline [37], warfarin [38] and caffeine [39], to mitigate potential risks. Additionally, ebselen may act as an inhibitor for CYP2C19 and CYP2C9; therefore, caution must be exercised when combining it with drugs reliant on liver drug enzymes' metabolism, like antidepressants [40] and warfarin [41]. Ebselen may also serve as a substrate for CYP3A4; however, since CYP3A4 metabolizes numerous drugs within the CYP450 system, additional precautions need to be considered to minimize associated risks by avoiding concurrent use with macrolides, antidepressants, anti-HIV medications, etc. [42].

This study was limited to in vitro conditions with artificially constructed viral proteins, underscoring the need for subsequent intracellular and animal studies to validate these findings. Future research should also aim to expand the repertoire of drugs tested to enhance the robustness of our drug screening system.

Acknowledgements

The authors thank all the colleagues of the Department of Clinical Laboratory for their comments on the earlier versions of this manuscript. We thank Tong Hongfang from the Endocrinology Department of Anhui Province, Mengcheng County People's Hospital for her hard work. This study received supporting from the Scientific Research Project of the Health Commission of Anhui Province (grant no. AHWJ2021a013) and the Anhui Medical University Clinical and Early Discipline Co-construction Project.

Disclosure of conflict of interest

None.

Address correspondence to: Dr. Wei Xu, Department of Blood Transfusion, The First Affiliated Hospital of Anhui Medical University, No. 210 Jixi Road, Hefei 230022, Anhui, PR China. E-mail: xuwei@ahmu.edu.cn; Dr. Mei Zhu, Department of Clinical Laboratory, The Affiliated Chaohu Hospital of Anhui Medical University, No. 64 Chaohu North Road, Chaohu 238000, Anhui, PR China. E-mail: zhumei@ahmu.edu.cn

References

[1] Wu JT, Leung K and Leung GM. Nowcasting and forecasting the potential domestic and international spread of the 2019-nCoV outbreak originating in Wuhan, China: a modelling study. Lancet 2020; 395: 689-697.

[2] Hui DS, I Azhar E, Madani TA, Ntoumi F, Kock R, Dar O, Ippolito G, Mchugh TD, Memish ZA, Drosten C, Zumla A and Petersen E. The continuing 2019-nCoV epidemic threat of novel coronaviruses to global health - The latest 2019 novel coronavirus outbreak in Wuhan, China. Int J Infect Dis 2020; 91: 264-266.

[3] Ioannidis JPA. Global perspective of COVID-19 epidemiology for a full-cycle pandemic. Eur J Clin Invest 2020; 50: e13423.

[4] da Costa VG, Moreli ML and Saivish MV. The emergence of SARS, MERS and novel SARS-2 coronaviruses in the 21st century. Arch Virol 2020; 165: 1517-1526.

[5] Khailany RA, Safdar M and Ozaslan M. Genomic characterization of a novel SARS-CoV-2. Gene Rep 2020; 19: 100682.
[6] Tam D, Lorenzo-Leal AC, Hernández LR and Bach H. Targeting SARS-CoV-2 non-structural proteins. Int J Mol Sci 2023; 24: 13002.
[7] Redondo N, Zaldívar-López S, Garrido JJ and Montoya M. SARS-CoV-2 accessory proteins in viral pathogenesis: knowns and unknowns. Front Immunol 2021; 12: 708264.
[8] Perlman S and Netland J. Coronaviruses post-SARS: update on replication and pathogenesis. Nat Rev Microbiol 2009; 7: 439-450.
[9] Deming DJ, Graham RL, Denison MR and Baric RS. Processing of open reading frame 1a replicase proteins nsp7 to nsp10 in murine hepatitis virus strain A59 replication. J Virol 2007; 81: 10280-10291.
[10] Eckerle LD, Lu X, Sperry SM, Choi L and Denison MR. High fidelity of murine hepatitis virus replication is decreased in nsp14 exoribonuclease mutants. J Virol 2007; 81: 12135-12144.
[11] Ivanov KA, Hertzig T, Rozanov M, Bayer S, Thiel V, Gorbalenya AE and Ziebuhr J. Major genetic marker of nidoviruses encodes a replicative endoribonuclease. Proc Natl Acad Sci U S A 2004; 101: 12694-12699.
[12] Hsu JC, Laurent-Rolle M, Pawlak JB, Wilen CB and Cresswell P. Translational shutdown and evasion of the innate immune response by SARS-CoV-2 NSP14 protein. Proc Natl Acad Sci U S A 2021; 118: e2101161118.
[13] Lei X, Dong X, Ma R, Wang W, Xiao X, Tian Z, Wang C, Wang Y, Li L, Ren L, Guo F, Zhao Z, Zhou Z, Xiang Z and Wang J. Activation and evasion of type I interferon responses by SARS-CoV-2. Nat Commun 2020; 11: 3810.
[14] Schindewolf C, Lokugamage K, Vu MN, Johnson BA, Scharton D, Plante JA, Kalveram B, Crocquet-Valdes PA, Sotcheff S, Jaworski E, Alvarado RE, Debbink K, Daugherty MD, Weaver SC, Routh AL, Walker DH, Plante KS and Menachery VD. SARS-CoV-2 uses nonstructural protein 16 to evade restriction by IFIT1 and IFIT3. J Virol 2023; 97: e0153222.
[15] Beyer DK and Forero A. Mechanisms of antiviral immune evasion of SARS-CoV-2. J Mol Biol 2022; 434: 167265.
[16] Chen Y and Guo D. Molecular mechanisms of coronavirus RNA capping and methylation. Virol Sin 2016; 31: 3-11.
[17] Czarna A, Plewka J, Kresik L, Matsuda A, Karim A, Robinson C, O'Byrne S, Cunningham F, Georgiou I, Wilk P, Pachota M, Popowicz G, Wyatt PG, Dubin G and Pyrć K. Refolding of lid subdomain of SARS-CoV-2 nsp14 upon nsp10 interaction releases exonuclease activity. Structure 2022; 30: 1050-1054, e2.
[18] Bobrovs R, Kanepe I, Narvaiss N, Patetko L, Kalnins G, Sisovs M, Bula AL, Grinberga S, Boroduskis M, Ramata-Stunda A, Rostoks N, Jirgensons A, Tars K and Jaudzems K. Discovery of SARS-CoV-2 nsp14 and nsp16 methyltransferase inhibitors by high-throughput virtual screening. Pharmaceuticals (Basel) 2021; 14: 1243.
[19] Sulimov A, Kutov D, Ilin I, Xiao Y, Jiang S and Sulimov V. Novel inhibitors of 2'-O-methyltransferase of the SARS-CoV-2 coronavirus. Molecules 2022; 27: 2721.
[20] Molica M, Breccia M, Capria S, Trisolini S, Foa R, Jabbour E and Kadia TM. The role of cladribine in acute myeloid leukemia: an old drug up to new tricks. Leuk Lymphoma 2020; 61: 536-545.
[21] Sigal DS, Miller HJ, Schram ED and Saven A. Beyond hairy cell: the activity of cladribine in other hematologic malignancies. Blood 2010; 116: 2884-2896.
[22] Nabizadeh F, Mohamadi M, Rahmani S, Rajabi R, Afrashteh F, Najdaghi S and Mirmosayyeb O. Safety and efficacy of cladribine in multiple sclerosis: a systematic review and meta-analysis. Neurol Sci 2023; 44: 3045-3057.
[23] Rejdak K, Szklener S, Korchut A and Baranowski D. Cladribine in myasthenia gravis: a pilot open-label study. Eur J Neurol 2020; 27: 586-589.
[24] Moreno S, Hernández B and Dronda F. Didanosine enteric-coated capsule: current role in patients with HIV-1 infection. Drugs 2007; 67: 1441-1462.
[25] Tazikeh-Lemeski E, Moradi S, Raoufi R, Shahlaei M, Janlou MAM and Zolghadri S. Targeting SARS-COV-2 non-structural protein 16: a virtual drug repurposing study. J Biomol Struct Dyn 2021; 39: 4633-4646.
[26] Pugh CS, Borchardt RT and Stone HO. Sinefungin, a potent inhibitor of virion mRNA(guanine-7-)-methyltransferase, mRNA(nucleoside-2'-)-methyltransferase, and viral multiplication. J Biol Chem 1978; 253: 4075-4077.
[27] Kasprzyk R, Fido M, Mamot A, Wanat P, Smietanski M, Kopcial M, Cowling VH, Kowalska J and Jemielity J. Direct high-throughput screening assay for mRNA cap guanine-N7 methyltransferase activity. Chemistry 2020; 26: 11266-11275.
[28] Khalili Yazdi A, Li F, Devkota K, Perveen S, Ghiabi P, Hajian T, Bolotokova A and Vedadi M. A high-throughput radioactivity-based assay for screening SARS-CoV-2 nsp10-nsp16 complex. SLAS Discov 2021; 26: 757-765.
[29] Sies H and Parnham MJ. Potential therapeutic use of ebselen for COVID-19 and other respiratory viral infections. Free Radic Biol Med 2020; 156: 107-112.

[30] Thenin-Houssier S, de Vera IM, Pedro-Rosa L, Brady A, Richard A, Konnick B, Opp S, Buffone C, Fuhrmann J, Kota S, Billack B, Pietka-Ottlik M, Tellinghuisen T, Choe H, Spicer T, Scampavia L, Diaz-Griffero F, Kojetin DJ and Valente ST. Ebselen, a small-molecule capsid inhibitor of HIV-1 replication. Antimicrob Agents Chemother 2016; 60: 2195-2208.

[31] Jin Z, Du X, Xu Y, Deng Y, Liu M, Zhao Y, Zhang B, Li X, Zhang L, Peng C, Duan Y, Yu J, Wang L, Yang K, Liu F, Jiang R, Yang X, You T, Liu X, Yang X, Bai F, Liu H, Liu X, Guddat LW, Xu W, Xiao G, Qin C, Shi Z, Jiang H, Rao Z and Yang H. Structure of M(pro) from SARS-CoV-2 and discovery of its inhibitors. Nature 2020; 582: 289-293.

[32] Xu L, Jiao J, Sun X, Sang W, Gao X, Yang P, Yan D, Song X, Sun C, Liu M, Qin Y, Tian Y, Zhu F, Zeng L, Li Z and Xu K. Cladribine induces ATF4 mediated apoptosis and synergizes with SAHA in diffuse large B-cell lymphoma cells. Int J Med Sci 2020; 17: 1375-1384.

[33] Haug SJ, Wong RW, Day S, Choudhry N, Sneed S, Prasad P, Read S, McDonald RH, Agarwal A, Davis J and Sarraf D. Didanosine retinal toxicity. Retina 2016; 36 Suppl 1: S159-S167.

[34] Ware AJ, Berggren RA and Taylor WE. Didanosine-induced hepatitis. Am J Gastroenterol 2000; 95: 2141-2143.

[35] Pattanaik A, Bhandarkar B S, Lodha L and Marate S. SARS-CoV-2 and the nervous system: current perspectives. Arch Virol 2023; 168: 171.

[36] Stein SR, Ramelli SC, Grazioli A, Chung JY, Singh M, Yinda CK, Winkler CW, Sun J, Dickey JM, Ylaya K, Ko SH, Platt AP, Burbelo PD, Quezado M, Pittaluga S, Purcell M, Munster VJ, Belinky F, Ramos-Benitez MJ, Boritz EA, Lach IA, Herr DL, Rabin J, Saharia KK, Madathil RJ, Tabatabai A, Soherwardi S, McCurdy MT; NIH COVID-19 Autopsy Consortium, Peterson KE, Cohen JI, de Wit E, Vannella KM, Hewitt SM, Kleiner DE and Chertow DS. SARS-CoV-2 infection and persistence in the human body and brain at autopsy. Nature 2022; 612: 758-763.

[37] Xiong S and Li L. The effect of CYP1A2 gene polymorphism on the metabolism of theophylline. Exp Ther Med 2018; 15: 109-114.

[38] Mar PL, Gopinathannair R, Gengler BE, Chung MK, Perez A, Dukes J, Ezekowitz MD, Lakkireddy D, Lip GYH, Miletello M, Noseworthy PA, Reiffel J, Tisdale JE and Olshansky B; from the American Heart Association Electrocardiography & Arrhythmias Committee of the Council of Clinical Cardiology. Drug interactions affecting oral anticoagulant use. Circ Arrhythm Electrophysiol 2022; 15: e007956.

[39] Vaynshteyn D and Jeong H. Caffeine induces CYP1A2 expression in rat hepatocytes but not in human hepatocytes. Drug Metab Lett 2012; 6: 116-119.

[40] Bousman CA, Stevenson JM, Ramsey LB, Sangkuhl K, Hicks JK, Strawn JR, Singh AB, Ruaño G, Mueller DJ, Tsermpini EE, Brown JT, Bell GC, Leeder JS, Gaedigk A, Scott SA, Klein TE, Caudle KE and Bishop JR. Clinical Pharmacogenetics Implementation Consortium (CPIC) guideline for CYP2D6, CYP2C19, CYP2B6, SLC6A4, and HTR2A genotypes and serotonin reuptake inhibitor antidepressants. Clin Pharmacol Ther 2023; 114: 51-68.

[41] Flora DR, Rettie AE, Brundage RC and Tracy TS. CYP2C9 genotype-dependent warfarin pharmacokinetics: impact of CYP2C9 genotype on R- and S-warfarin and their oxidative metabolites. J Clin Pharmacol 2017; 57: 382-393.

[42] Zhou SF. Drugs behave as substrates, inhibitors and inducers of human cytochrome P450 3A4. Curr Drug Metab 2008; 9: 310-322.

Table S1. The ADMET profile of cladribine, didanosine, sinefungin and ebselen

Explanation of available endpoints
(1) Physicochemical Property

Molecular Weight

Contain hydrogen atoms. Optimal: 100-600, based on Drug-Like soft rule.

Volume

van der Waals volume.

Density

Density = MW/volume.

nHA

Number of hydrogen bond acceptors. Sum of all o and N. Optimal: 0-12, based on Drug-Like soft rule.

nHD

Number of hydrogen bond donors. Sum of all OHs and NHs. Optimal: 0-7, based on Drug-Like soft rule.

nRot

Number of rotatable bonds. In some situation Amide C-N bonds are not considered because of their high rotational energy barrier. Optimal: 0-11, based on Drug-Like soft rule.

nRing

Number of rings. Smallest set of smallest rings. Optimal: 0-6, based on Drug-Like soft rule.

MaxRing

Number of atoms in the biggest ring. Number of atoms involved in the biggest system ring. Optimal: 0-18, based on Drug-Like soft rule.

nHet

Number of heteroatoms. Number of non-carbon atoms (hydrogens included). Optimal: 1-15, based on Drug-Like soft rule.

fChar

Formal charge. Optimal: -4-4, based on Drug-Like soft rule.

nRig

Number of rigid bonds. Number of non-flexible bonds, in opposite to rotatable bonds. Optimal: 0-30, based on Drug-Like soft rule.

Flexibility

Flexibility = nRot/nRig.

Stereo Centers

Number of stereocenters. Optimal: < 2, based on Lead-Like soft rule.

TPSA

Topological polar surface area. Sum of tabulated surface contributions of polar fragments. Optimal: 0-140, based on veber rule.

logS

- The logarithm of aqueous solubility value. The first step in the drug absorption process is the disintegration of the tablet or capsule, followed by the dissolution of the active drug. Low solubility is detrimental to good and complete oral absorption, and early measurement of this property is of great importance in drug discovery.
- Results interpretation: The predicted solubility of a compound is given as the logarithm of the molar concentration (log mol/L). Compounds in the range from -4 to 0.5 log mol/L will be considered proper.

logP

- The logarithm of the n-octanol/water distribution coefficient. logP possess a leading position with considerable impact on both membrane permeability and hydrophobic binding to macromolecules, including the target receptor as well as other proteins like plasma proteins, transporters, or metabolizing enzymes.
- Results interpretation: The predicted logP of a compound is given as the logarithm of the molar concentration (log mol/L). Compounds in the range from 0 to 3 log mol/L will be considered proper.

logD7.4

- The logarithm of the n-octanol/water distribution coefficients at pH = 7.4. To exert a therapeutic effect, one drug must enter the blood circulation and then reach the site of action. Thus, an eligible drug usually needs to keep a balance between lipophilicity and hydrophilicity to dissolve in the body fluid and penetrate the biomembrane effectively. Therefore, it is important to estimate the n-octanol/water distribution coefficients at physiological pH (logD7.4) values for candidate compounds in the early stage of drug discovery.
- Results interpretation: The predicted logD7.4 of a compound is given as the logarithm of the molar concentration (log mol/L). Compounds in the range from 1 to 3 log mol/L will be considered proper.

(2) Medicinal Chemistry

QED

- A measure of drug-likeness based on the concept of desirability. QED is calculated by integrating the outputs of the desirability functions based on eight drug-likeness related properties, including MW, logP, NHBA, NHBD, PSA, Nrotb, the number of aromatic rings (NAr), and the number of alerts for undesirable functional groups. Here, average descriptor weights were used in the calculation of QED. The QED score is calculated by taking the geometric mean of the individual desirability functions, given by QED = exp $(\frac{1}{n}\sum_{i=1}^{n} \ln d_i)$, where d_i indicates the dth desirability function and n = 8 is the number of drug-likeness related properties.
- Results interpretation: The mean QED is 0.67 for the attractive compounds, 0.49 for the unattractive compounds and 0.34 for the unattractive compounds considered too complex.
- Empirical decision: > 0.67: excellent (green); < 0.67: poor (red).

SAscore

- Synthetic accessibility score is designed to estimate ease of synthesis of drug-like molecules, based on a combination of fragment contributions and a complexity penalty. The score is between 1 (easy to make) and 10 (very difficult to make). The synthetic accessibility score (SAscore) is calculated as a combination of two components: AScoTe = fTagmentScoTe - complexityPenalty.
- Results interpretation: high SAscore: > 6, difficult to synthesize; low SAscore: < 6, easy to synthesize.
- Empirical decision: < 6: excellent (green); > 6: poor (red).

Fsp3

- Fsp3, the number of sp3 hybridized carbons/total carbon count, is used to determine the carbon saturation of molecules and characterize the complexity of the spatial structure of molecules. It has been demonstrated that the increased saturation measured by Fsp3 and the number of chiral centers in the molecule increase the clinical success rate, which might be related to the increased solubility, or the fact that the enhanced 3D features allow small molecules to occupy more target space.
- Results interpretation: Fsp3 > 0.42 is considered a suitable value.
- Empirical decision: > 0.42: excellent (green); < 0.42: poor (red).

MCE-18

- MCE-18 stands for medicinal chemistry evolution in 2018, and this measure can effectively score molecules by novelty in terms of their cumulative sp3 complexity. It can effectively score structures by their novelty and current lead potential in contrast to simple and in many cases false positive sp3 index, and given by the following equation: MCE18 = (AR + NAR + CHIRAL + SPIRO + $\frac{sp^3 + Cyc - Acyc}{1 + sp^3}$) ×Q1, where AR is the presence of an aromatic or heteroaromatic ring (0 or 1), NAR is the presence of an aliphatic or a heteroaliphatic ring (0 or 1), cHIRAL is the presence of a chiral center (0 or 1), SpIRO is the presence of a spiro point (0 or 1), sp3 is the portion of sp3-hybridized carbon atoms (from 0 to 1), cyc is the portion of cyclic carbons that are sp3 hybridized (from 0 to 1), Acyc is a portion of acyclic carbon atoms that are sp3 hybridized (from 0 to 1), and Q1 is the normalized quadratic index.
- Results interpretation: < 45: uninteresting, trivial, old scaffolds, low degree of 3D complexity and novelty; 45-63: sufficient novelty, basically follow the trends of currently observed in medicinal chemistry; 63-78: high structural similarity to the compounds disclosed in patent records; > 78: need to be inspected visually to assess their target profile and drug-likeness.
- Empirical decision: > 45: excellent (green); < 45: poor (red).

NPscore

- The Natural product-likeness score is a useful measure which can help to guide the design of new molecules toward interesting regions of chemical space which have been identified as “bioactive regions” by natural evolution. The calculation consists of molecule fragmentation, table lookup, and summation of fragment contributions.
- Results interpretation: The calculated score is typically in the range from -5 to 5. The higher the score is, the higher the probability is that the molecule is a Np.

Lipinski Rule

- Content: MW < 500; logP < 5; Hacc < 10; Hdon < 5.
- Results interpretation: If two properties are out of range, a poor absorption or permeability is possible, one is acceptable.
- Empirical decision: < 2 violations: excellent (green); > 2 violations: poor (red).

Pfizer Rule

- Content: logP > 3; TPSA < 75.
- Results interpretation: Compounds with a high logP (> 3) and low TPSA (< 75) are likely to be toxic.
- Empirical decision: two conditions satisfied: poor (red); otherwise: excellent (green).

GSK Rule

- Content: MW < 400; logP < 4.
- Results interpretation: Compounds satisfying the GSK rule may have a more favorable ADMET profile.
- Empirical decision: 0 violation: excellent (green); otherwise: poor (red).

Golden Triangle

- Content: 200 < MW < 50; -2 < logD < 5.
- Results interpretation: Compounds satisfying the GoldenTriangle rule may have a more favourable ADMET profile.
- Empirical decision: 0 violation: excellent (green); otherwise: poor (red).

(3) Absorption

Caco-2 Permeability

- Before an oral drug reaches the systemic circulation, it must pass through intestinal cell membranes via passive diffusion, carrier-mediated uptake or active transport processes. The human colon adenocarcinoma cell lines (caco-2), as an alternative approach for the human intestinal epithelium, has been commonly used to estimate in vivo drug permeability due to their morphological and functional similarities. Thus, caco-2 cell permeability has also been an important index for an eligible candidate drug compound.
- Results interpretation: The predicted caco-2 permeability of a given compound is given as the log cm/s. A compound is considered to have a proper cao-2 permeability if it has predicted value > -5.15 log cm/s.
- Empirical decision: > -5.15: excellent (green); otherwise: poor (red).

MDCK Permeability

- Madin-Darby canine Kidney cells (MDCK) have been developed as an in vitro model for permeability screening. Its apparent permeability coefficient, P_{app}, is widely considered to be the in vitro gold standard for assessing the uptake efficiency of chemicals into the body. P_{app} values of MDCK cell lines are also used to estimate the effect of the blood-brain barrier (BBB).
- Results interpretation: The unit of predicted MDCK permeability is cm/s. A compound is considered to have a high passive MDCK permeability for a $P_{app} > 20\times10^{-6}$ cm/s, medium permeability for $2\text{-}20\times10^{-6}$ cm/s, low permeability for $< 2\times10^{-6}$ cm/s.
- Empirical decision: $> 2\times10^{-6}$ cm/s: excellent (green); otherwise: poor (red).

Pgp-Inhibitor

- The inhibitor of p-glycoprotein. The p-glycoprotein, also known as MDR1 or 2 ABcB1, is a membrane protein member of the ATP-binding cassette (ABc) transporters superfamily. It is probably the most promiscuous efflux transporter, since it recognizes a number of structurally different and apparently unrelated xenobiotics; notably, many of them are also cyp3A4 substrates.
- Results interpretation: category 0: Non-inhibitor; category 1: Inhibitor. The output value is the probability of being Pgp-inhibitor, within the range of 0 to 1.
- Empirical decision: 0-0.3: excellent (green); 0.3-0.7: medium (yellow); 0.7-1.0 (++): poor (red).

Pgp-Substrate

- As described in the Pgp-inhibitor section, modulation of p-glycoprotein mediated transport has significant pharmacokinetic implications for Pgp substrates, which may either be exploited for specific therapeutic advantages or result in contraindications.
- Results interpretation: category 0: Non-substrate; category 1: Substrate. The output value is the probability of being Pgp-substrate, within the range of 0 to 1.
- Empirical decision: 0-0.3: excellent (green); 0.3-0.7: medium (yellow); 0.7-1.0 (++): poor (red).

HIA

- Human intestinal absorption. As described above, the human intestinal absorption of an oral drug is the essential prerequisite for its apparent efficacy. What's more, the close relationship between oral bioavailability and intestinal absorption has also been proven and HIA can be seen an alternative indicator for oral bioavailability to some extent.
- Result interpretation: A molecule with an absorbance of less than 30% is considered to be poorly absorbed. Accordingly, molecules with a HIA > 30% were classified as HIA- (category 0), while molecules with a HIA < 30% were classified as HIA+ (category 1). The output value is the probability of being HIA+, within the range of 0 to 1.
- Empirical decision: 0-0.3: excellent (green); 0.3-0.7: medium (yellow); 0.7-1.0 (++): poor (red).

F20%

- The human oral bioavailability 20%. For any drug administrated by the oral route, oral bioavailability is undoubtedly one of the most important pharmacokinetic parameters because it is the indicator of the efficiency of the drug delivery to the systemic circulation.
- Result interpretation: Molecules with a bioavailability > 20% were classified as F20%- (category 0), while molecules with a bioavailability < 20% were classified as F20%+ (category 1). The output value is the probability of being F20%+, within the range of 0 to 1.
- Empirical decision: 0-0.3: excellent (green); 0.3-0.7: medium (yellow); 0.7-1.0 (++): poor (red).

F30%

- The human oral bioavailability 30%. For any drug administrated by the oral route, oral bioavailability is undoubtedly one of the most important pharmacokinetic parameters because it is the indicator of the efficiency of the drug delivery to the systemic circulation.
- Result interpretation: Molecules with a bioavailability > 30% were classified as F30%- (category 0), while molecules with a bioavailability < 30% were classified as F30%+ (category 1). The output value is the probability of being F30%+, within the range of 0 to 1.
- Empirical decision: 0-0.3: excellent (green); 0.3-0.7: medium (yellow); 0.7-1.0 (++): poor (red).

(4) Distribution

PPB

- Plasma protein binding. One of the major mechanisms of drug uptake and distribution is through PPB, thus the binding of a drug to proteins in plasma has a strong influence on its pharmacodynamic behavior. PPB can directly influence the oral bioavailability because the free concentration of the drug is at stake when a drug binds to serum proteins in this process.
- Result interpretation: A compound is considered to have a proper PPB if it has predicted value < 90%, and drugs with high protein-bound may have a low therapeutic index.
- Empirical decision: < 90%: excellent (green); otherwise: poor (red).

VD

- Volume Distribution. The VD is a theoretical concept that connects the administered dose with the actual initial concentration present in the circulation and it is an important parameter to describe the in vivo distribution for drugs. In practice, we can speculate the distribution characters for an unknown compound according to its VD value, such as its condition binding to plasma protein, its distribution amount in body fluid and its uptake amount in tissues.
- Result interpretation: The unit of predicted VD is L/kg. A compound is considered to have a proper VD if it has predicted VD in the range of 0.04-20 L/kg.
- Empirical decision: 0.04-20: excellent (green); otherwise: poor (red).

BBB Penetration

- Drugs that act in the cNS need to cross the blood-brain barrier (BBB) to reach their molecular target. By contrast, for drugs with a peripheral target, little or no BBB penetration might be required in order to avoid cNS side effects.
- Result interpretation: The unit of BBB penetration is cm/s. Molecules with logBB > -1 were classified as BBB+ (category 1), while molecules with logBB < -1 were classified as BBB- (category 0). The output value is the probability of being BBB+, within the range of 0 to 1.
- Empirical decision: 0-0.3: excellent (green); 0.3-0.7: medium (yellow); 0.7-1.0 (++): poor (red).

Fu

- The fraction unbound in plasms. Most drugs in plasma will exist in equilibrium between either an unbound state or bound to serum proteins. Efficacy of a given drug may be affect by the degree to which it binds proteins within blood, as the more that is bound the less efficiently it can traverse cellular membranes or diffuse.

- Result interpretation: > 20%: High Fu; 5-20%: medium Fu; < 5%: low Fu.
- Empirical decision: > 5%: excellent (green); < 5%: poor (red).

(5) Metabolism

CYP1A2/2C19/2C9/2D6/3A4 inhibitor

CYP1A2/2C19/2C9/2D6/3A4 substrate

- Based on the chemical nature of biotransformation, the process of drug metabolism reactions can be divided into two broad categories: phase I (oxidative reactions) and phase II (conjugative reactions). The human cytochrome P450 family (phase I enzymes) contains 57 isozymes and these isozymes metabolize approximately two-thirds of known drugs in human with 80% of this attribute to five isozymes - 1A2, 3A4, 2c9, 2c19 and 2D6. Most of these cyPs responsible for phase I reactions are concentrated in the liver.
- Result interpretation: category 0: Non-substrate/Non-inhibitor; category 1: Substrate/Inhibitor. The output value is the probability of being substrate/inhibitor, within the range of 0 to 1.

(6) Excretion

CL

- The clearance of a drug. Clearance is an important pharmacokinetic parameter that defines, together with the volume of distribution, the half-life, and thus the frequency of dosing of a drug.
- Result interpretation: The unit of predicted CL penetration is ml/min/kg. > 15 ml/min/kg: high clearance; 5-15 ml/min/kg: moderate clearance; < 5 ml/min/kg: low clearance.
- Empirical decision: > 5: excellent (green); < 5: poor (red).

$T_{1/2}$

- The half-life of a drug is a hybrid concept that involves clearance and volume of distribution, and it is arguably more appropriate to have reliable estimates of these two properties instead.
- Result interpretation: Molecules with $T_{1/2}$ > 3 were classified as $T_{1/2}$- (category 0), while molecules with $T_{1/2}$ < 3 were classified as $T_{1/2}$+ (category 1). The output value is the probability of being $T_{1/2}$+, within the range of 0 to 1.
- Empirical decision: 0-0.3: excellent (green); 0.3-0.7: medium (yellow); 0.7-1.0 (++): poor (red).

(7) Toxicology

hERG Blockers

- The human ether-a-go-go related gene. During cardiac depolarization and repolarization, a voltage-gated potassium channel encoded by hERG plays a major role in the regulation of the exchange of cardiac action potential and resting potential. The hERG blockade may cause long QT syndrome (LQTS) arrhythmia, and Torsade de pointes (Tdp), which lead to palpitations, fainting, or even sudden death.
- Result interpretation: Molecules with Ic_{50} more than 10 μM or less than 50% inhibition at 10 μM were classified as hERG- (category 0), while molecules with Ic_{50} less than 10 μM or more than 50% inhibition at 10 μM were classified as hERG+ (category 1). The output value is the probability of being hERG+, within the range of 0 to 1.
- Empirical decision: 0-0.3: excellent (green); 0.3-0.7: medium (yellow); 0.7-1.0 (++): poor (red).

H-HT

- The human hepatotoxicity. Drug induced liver injury is of great concern for patient safety and a major cause for drug withdrawal from the market. Adverse hepatic effects in clinical trials often lead to a late and costly termination of drug development programs.
- Result interpretation: category 0: H-HT negative (-); category 1: H-HT positive (+). The output value is the probability of being toxic, within the range of 0 to 1.
- Empirical decision: 0-0.3: excellent (green); 0.3-0.7: medium (yellow); 0.7-1.0 (++): poor (red).

DILI

- Drug-induced liver injury (DILI) has become the most common safety problem of drug withdrawal from the market over the past 50 years.
- Result interpretation: category 0: DILI negative (-); category 1: DILI positive (+). The output value is the probability of being toxic, within the range of 0 to 1.
- Empirical decision: 0-0.3: excellent (green); 0.3-0.7: medium (yellow); 0.7-1.0 (++): poor (red).

AMES Toxicity

- The Ames test for mutagenicity. The mutagenic effect has a close relationship with the carcinogenicity, and it is the most widely used assay for testing the mutagenicity of compounds.
- Result interpretation: category 0: AMES negative (-); category 1: AMES positive (+). The output value is the probability of being toxic, within the range of 0 to 1.

- Empirical decision: 0-0.3: excellent (green); 0.3-0.7: medium (yellow); 0.7-1.0 (++): poor (red).

Rat Oral Acute Toxicity

- Determination of acute toxicity in mammals (e.g. rats or mice) is one of the most important tasks for the safety evaluation of drug candidates.
- Result interpretation: category 0: low-toxicity, > 500 mg/kg; category 1: high-toxicity, < 500 mg/kg. The output value is the probability of being toxic, within the range of 0 to 1.
- Empirical decision: 0-0.3: excellent (green); 0.3-0.7: medium (yellow); 0.7-1.0 (++): poor (red).

FDAMDD

- The maximum recommended daily dose provides an estimate of the toxic dose threshold of chemicals in humans.
- Result interpretation: category 1: FDAMDD positive (+), < 0.011 mmol/kg-bw/day; category 0: FDAMDD negative (-), > 0.011 mmol/kg-bw/day. The output value is the probability of being toxic, within the range of 0 to 1.
- Empirical decision: 0-0.3: excellent (green); 0.3-0.7: medium (yellow); 0.7-1.0 (++): poor (red).

Skin Sensitization

- Skin sensitization is a potential adverse effect for dermally applied products. The evaluation of whether a compound, that may encounter the skin, can induce allergic contact dermatitis is an important safety concern.
- Result interpretation: category 1: Sensitizer; category 0: Non-sensitizer. The output value is the probability of being toxic, within the range of 0 to 1.
- Empirical decision: 0-0.3: excellent (green); 0.3-0.7: medium (yellow); 0.7-1.0 (++): poor (red).

Carcinogenicity

- Among various toxicological endpoints of chemical substances, carcinogenicity is of great concern because of its serious effects on human health. The carcinogenic mechanism of chemicals may be due to their ability to damage the genome or disrupt cellular metabolic processes. Many approved drugs have been identified as carcinogens in humans or animals and have been withdrawn from the market.
- Result interpretation: category 1: carcinogens; category 0: non-carcinogens. Chemicals are labelled as active (carcinogens) or inactive (non-carcinogens) according to their TD50 values. The output value is the probability of being toxic, within the range of 0 to 1.
- Empirical decision: 0-0.3: excellent (green); 0.3-0.7: medium (yellow); 0.7-1.0 (++): poor (red).

Eye Corrosion/Irritation

- Assessing the eye irritation/corrosion (Ei/Ec) potential of a chemical is a necessary component of risk assessment. Cornea and conjunctiva tissues comprise the anterior surface of the eye, and hence cornea and conjunctiva tissues are directly exposed to the air and easily suffer injury by chemicals. There are several substances, such as chemicals used in manufacturing, agriculture and warfare, ocular pharmaceuticals, cosmetic products, and household products, that can cause Ei or Ec.
- Result interpretation: category 1: corrosives/irritants chemicals; category 0: non-corrosives/non-irritants chemicals. The output value is the probability of being toxic, within the range of 0 to 1.
- Empirical decision: 0-0.3: excellent (green); 0.3-0.7: medium (yellow); 0.7-1.0 (++): poor (red).

Respiratory Toxicity

- Among these safety issues, respiratory toxicity has become the main cause of drug withdrawal. Drug induced respiratory toxicity is usually underdiagnosed because it may not have distinct early signs or symptoms in common medications and can occur with significant morbidity and mortality. Therefore, careful surveillance and treatment of respiratory toxicity is of great importance.
- Result interpretation: category 1: respiratory toxicants; category 0: non-respiratory toxicants. The output value is the probability of being toxic, within the range of 0 to 1.
- Empirical decision: 0-0.3: excellent (green); 0.3-0.7: medium (yellow); 0.7-1.0 (++): poor (red).

Bioconcentration Factor

- The Bioconcentration factor (BcF) is defined as the ratio of the chemical concentration in biota as a result of absorption via the respiratory surface to that in water at steady state. It is used for considering secondary poisoning potential and assessing risks to human health via the food chain. The unit of BcF is log10 (L/kg).

IGC50

- 48 hour Tetrahymena pyriformis IGC50 (concentration of the test chemical in water in mg/L that causes 50% growth inhibition to Tetrahymena pyriformis after 48 hours). The unit of IGC50 is -log10[(mg/L)/(1000*MW)].

LC50FM

- 96 hour fathead minnow LC50 (concentration of the test chemical in water in mg/L that causes 50% of fathead minnow to die after 96 hours). The unit of LC50FM is -log10[(mg/L)/(1000*MW)].

LC50DM

- 48 hour Daphnia magna LC50 (concentration of the test chemical in water in mg/L that causes 50% of Daphnia magna to die after 48 hours). The unit of LC50DM is -log10[(mg/L)/(1000*MW)].

NR-AR

- Androgen receptor (AR), a nuclear hormone receptor, plays a critical role in AR-dependent prostate cancer and other androgen related diseases. Endocrine disrupting chemicals (EDCs) and their interactions with steroid hormone receptors like AR may cause disruption of normal endocrine function as well as interfere with metabolic homeostasis, reproduction, developmental and behavioral functions.
- Result interpretation: category 1: actives; category 0: inactives. The output value is the probability of being AR agonists, within the range of 0 to 1.
- Empirical decision: 0-0.3: excellent (green); 0.3-0.7: medium (yellow); 0.7-1.0 (++): poor (red).

NR-AR-LBD

- Androgen receptor (AR), a nuclear hormone receptor, plays a critical role in AR-dependent prostate cancer and other androgen related diseases. Endocrine disrupting chemicals (EDCs) and their interactions with steroid hormone receptors like AR may cause disruption of normal endocrine function as well as interfere with metabolic homeostasis, reproduction, developmental and behavioral functions.
- Result interpretation: category 1: actives; category 0: inactives. Molecules that labeled 1 in this bioassay may bind to the LBD of androgen receptor. The output value is the probability of being active, within the range of 0 to 1.
- Empirical decision: 0-0.3: excellent (green); 0.3-0.7: medium (yellow); 0.7-1.0 (++): poor (red).

NR-AhR

- The Aryl hydrocarbon Receptor (AhR), a member of the family of basic helix-loop-helix transcription factors, is crucial to adaptive responses to environmental changes. AhR mediates cellular responses to environmental pollutants such as aromatic hydrocarbons through induction of phase I and II enzymes but also interacts with other nuclear receptor signaling pathways.
- Result interpretation: category 1: actives; category 0: inactives. Molecules that labeled 1 may activate the aryl hydrocarbon receptor signaling pathway. The output value is the probability of being active, within the range of 0 to 1.
- Empirical decision: 0-0.3: excellent (green); 0.3-0.7: medium (yellow); 0.7-1.0 (++): poor (red).

NR-Aromatase

- Endocrine disrupting chemicals (EDcs) interfere with the biosynthesis and normal functions of steroid hormones including estrogen and androgen in the body. Aromatase catalyzes the conversion of androgen to estrogen and plays a key role in maintaining the androgen and estrogen balance in many of the EDc-sensitive organs.
- Result interpretation: category 1: actives; category 0: inactives. Molecules that labeled 1 are regarded as aromatase inhibitors that could affect the balance between androgen and estrogen. The output value is the probability of being active, within the range of 0 to 1.
- Empirical decision: 0-0.3: excellent (green); 0.3-0.7: medium (yellow); 0.7-1.0 (++): poor (red).

NR-ER

- Estrogen receptor (ER), a nuclear hormone receptor, plays an important role in development, metabolic homeostasis and reproduction. Endocrine disrupting chemicals (EDCS) and their interactions with steroid hormone receptors like ER causes disruption of normal endocrine function. Therefore, it is important to understand the effect of environmental chemicals on the ER signaling pathway.
- Result interpretation: category 1: actives; category 0: inactives. The output value is the probability of being active within the range of 0 to 1.
- Empirical decision: 0-0.3: excellent (green); 0.3-0.7: medium (yellow); 0.7-1.0 (++): poor (red).

NR-ER-LBD

- Estrogen receptor (ER), a nuclear hormone receptor, plays an important role in development, metabolic homeostasis and reproduction. Two subtypes of ER, ER-alpha and ER-beta have similar expression patterns with some uniqueness in both types. Endocrine disrupting chemicals (EDCS) and their interactions with steroid hormone receptors like ER causes disruption of normal endocrine function.

- Result interpretation: category 1: actives; category 0: inactives. The output value is the probability of being active within the range of 0 to 1.
- Empirical decision: 0-0.3: excellent (green); 0.3-0.7: medium (yellow); 0.7-1.0 (++): poor (red).

NR-PPAR-Gamma

- The peroxisome proliferator-activated receptors (PPARs) are lipid-activated transcription factors of the nuclear receptor superfamily with three distinct subtypes namely PPAR alpha, PPAR delta (also called PPAR beta) and PPAR gamma (PPARg). All these subtypes heterodimerize with Retinoid X receptor (RXR) and these heterodimers regulate transcription of various genes. PPAR-gamma receptor (glitazone receptor) is involved in the regulation of glucose and lipid metabolism.
- Result interpretation: category 1: actives; category 0: inactives. The output value is the probability of being active within the range of 0 to 1.
- Empirical decision: 0-0.3: excellent (green); 0.3-0.7: medium (yellow); 0.7-1.0 (++): poor (red).

SR-ARE

- Oxidative stress has been implicated in the pathogenesis of a variety of diseases ranging from cancer to neurodegeneration. The antioxidant response element (ARE) signaling pathway plays an important role in the amelioration of oxidative stress. The cellSensor ARE-bla HepG2 cell line (Invitrogen) can be used for analyzing the Nrf2/antioxidant response signaling pathway. Nrf2 (NF-E2-related factor 2) and Nrf1 are transcription factors that bind to AREs and activate these genes.
- Result interpretation: category 1: actives; category 0: inactives. The output value is the probability of being active within the range of 0 to 1.
- Empirical decision: 0-0.3: excellent (green); 0.3-0.7: medium (yellow); 0.7-1.0 (++): poor (red).

SR-ATAD5

- ATPase family AAA domain-containing protein 5. As cancer cells divide rapidly and during every cell division they need to duplicate their genome by DNA replication. The failure to do so results in the cancer cell death. Based on this concept, many chemotherapeutic agents were developed but have limitations such as low efficacy and severe side effects etc. Enhanced Level of Genome Instability Gene 1 (ELG1; human ATAD5) protein levels increase in response to various types of DNA damage.
- Result interpretation: category 1: actives; category 0: inactives. The output value is the probability of being active within the range of 0 to 1.
- Empirical decision: 0-0.3: excellent (green); 0.3-0.7: medium (yellow); 0.7-1.0 (++): poor (red).

SR-HSE

- Heat shock factor response element. Various chemicals, environmental and physiological stress conditions may lead to the activation of heat shock response/unfolded protein response (HSR/UPR). There are three heat shock transcription factors (HSFs) (HSF-1, -2, and -4) mediating transcriptional regulation of the human HSR.
- Result interpretation: category 1: actives; category 0: inactives. The output value is the probability of being active within the range of 0 to 1.
- Empirical decision: 0-0.3: excellent (green); 0.3-0.7: medium (yellow); 0.7-1.0 (++): poor (red).

SR-MMP

- Mitochondrial membrane potential (MMP), one of the parameters for mitochondrial function, is generated by mitochondrial electron transport chain that creates an electrochemical gradient by a series of redox reactions. This gradient drives the synthesis of ATP, a crucial molecule for various cellular processes. Measuring MMP in living cells is commonly used to assess the effect of chemicals on mitochondrial function; decreases in MMP can be detected using lipophilic cationic fluorescent dyes.
- Result interpretation: category 1: actives; category 0: inactives. The output value is the probability of being active within the range of 0 to 1.
- Empirical decision: 0-0.3: excellent (green); 0.3-0.7: medium (yellow); 0.7-1.0 (++): poor (red).

SR-p53

- p53, a tumor suppressor protein, is activated following cellular insult, including DNA damage and other cellular stresses. The activation of p53 regulates cell fate by inducing DNA repair, cell cycle arrest, apoptosis, or cellular senescence. The activation of p53, therefore, is a good indicator of DNA damage and other cellular stresses.
- Result interpretation: category 1: actives; category 0: inactives. The output value is the probability of being active within the range of 0 to 1.
- Empirical decision: 0-0.3: excellent (green); 0.3-0.7: medium (yellow); 0.7-1.0 (++): poor (red).